



Adsorption of Methylene blue and Methyl orange on tamarind seed activated carbon and its composite with chitosan: equilibrium and kinetic studies

Abdul Samad Kamdod, Malladi V Pavan Kumar*

Department of Chemical Engineering, National Institute of Technology Calicut, Kerala, India – 673601, Tel. +91-9746920959; emails: malladi@nitc.ac.in (M.V. Pavan Kumar), abdulsamad_p180007ch@nitc.ac.in (A.S. Kamdod)

Received 8 October 2021; Accepted 3 February 2022

ABSTRACT

Activated carbons were prepared from tamarind seed biomass (TSAC), and a composite of chitosan and the activated carbon was synthesized (CHS-TSAC). The two materials were tested for the adsorption of two dyes, namely Methylene blue (MB) and Methyl orange (MO), from their aqueous solutions. The two adsorbents were characterized using scanning electron microscopy, energy-dispersive X-ray, X-ray diffraction, Fourier-transform infrared spectroscopy, and Brunauer–Emmett–Teller. For batch adsorption experiments, the salient batch adsorption parameters, namely pH, adsorbent dosage, initial concentration, and contact time, were optimized in a sequential manner. For MB and MO, the optimal pH values were 10 and 3, respectively for both the adsorbents. A maximum adsorption capacity of 142.12 mg/g was seen for MB using TSAC. While, for MO, a maximum adsorption capacity of 94.45 mg/g was obtained using CHS-TSAC. Equilibrium adsorption data was experimentally obtained and successfully fitted for four nonlinear isotherm models. For all the cases, the equilibrium data and adsorption kinetics were best described by the Langmuir isotherm model and pseudo-second-order kinetics, respectively. In the regeneration studies, no significant loss in the adsorption capacity was observed for the tested three adsorption–desorption cycles.

Keywords: Activated carbon; Chitosan; Methylene blue; Methyl orange; Adsorption isotherm; Adsorption kinetics

1. Introduction

Owing to the use and discharge of synthetic dyes worldwide, water bodies are getting polluted rapidly, causing a severe threat to all forms of life. Apart from the increase of chemical oxygen demand and biochemical oxygen demand values of the contaminated waters, the presence of dyes in aquatic ecosystems can adversely affect the photosynthetic activity of aquatic plants and phytoplankton by reducing the transmission of sunlight [1–4]. The harmful effects of dyes and pigments on human health include itching, DNA mutation, dermatological diseases, liver and kidney damage, the disorderliness of the central nervous system, etc. It is estimated that about 90% of the water pollution is caused by organic chemicals, of which more than 50% is

attributed to dyes. Other organic chemicals include cosmetics, pigments, pharmaceutical products, hazardous hydrocarbons, pesticides, etc. [5,6]. The highly coloured waters are generally discharged from industries such as pulp and paper, textile, and dye manufacturing [7].

Methylene blue or MB ($C_{16}H_{18}ClN_3S$, M.W.: 319.859, cationic) and Methyl orange or MO ($C_{14}H_{14}N_3NaO_3S$, M.W.: 327.34, mono-azo anionic dye) are the most commonly used dyes in the textile industry and medical applications. These two dyes were reported to be toxic [8]. As MO is very resistant to degradation by heat, light, and several chemicals, excess energy is required for the conversion to non-harmful compounds [9,10]. As MB and MO cannot be removed naturally from the contaminated waters, efficient and cost-effective techniques are needed for their removal.

* Corresponding author.

Among the several methods and techniques available, adsorption is more economical with higher efficiencies, ease of use, low energy consumption, and no secondary pollution [11–14]. For MO removal, de-oiled soya and the bottom ash of a thermal power plant were successfully tested as adsorbents [11]. Recently, an ordered mesoporous carbon material was successfully utilized as an adsorbent for the removal of MO [8] and MB [15]. A magnetic cerium-organic framework-activated carbon composite [14], an iron-based metal-organic framework, and activated carbon prepared from waste tire were successfully tested for the adsorptive removal of MB [12,13].

The properties of the adsorbents are very crucial in their selection for the treatment. In recent years, attention is more focused on the development of novel adsorbents of the desirable properties such as maximum adsorption capacity, eco-friendliness, as well as a high degree of purification, etc., for the removal of dyes [16]. Crystal violet dye was separated from its aqueous solution using a bio-nano composite [17] and an iron-benzene dicarboxylic acid metal-organic framework [18], and this framework was doped with cobalt in another study and tested for the removal of Methylene blue [13]. Metal-organic frameworks are known for their tunable pore sizes and greater surface areas. A metal-halide-free ordered mesoporous carbon of very high specific surface area and larger pore volume was tested for the removal of the dyes, namely MO [8], Chrysoidine R [19,20], and Methylene blue [15] from their aqueous solutions. For wastewater treatment, especially for dyes removal, layered double hydroxides or anionic clays were recommended as adsorbents due to their stability, larger surface area, homogeneous charge distribution, and versatility to synthesize a variety of composites [21]. Researchers also attempted the development of activated carbons [22] and composites based on activated carbon for the removal of dyes [23].

Since commercial activated carbons are expensive, the development of adsorbents using biomass of insignificant economic value has attracted great attention in recent years. In this work, activated carbons were prepared from tamarind seeds (TSAC), and a composite, denoted as CHS-TSAC, was synthesized using TSAC and chitosan (CHS). Both TSAC and CHS-TSAC were tested for the adsorptive removal of two dyes (MB and MO) from their aqueous solutions. CHS is well known for its properties such as higher adsorption ability, biocompatibility, spectral sensitivity, and biodegradability [24,25]. Due to the presence of amino ($-\text{NH}_2$) and hydroxyl ($-\text{OH}$) groups in its molecular structure, CHS can easily adsorb dyes [26]. However, the disadvantages of CHS, such as lower mechanical strength, lower surface area, and higher swelling index, hinder its use in the unmodified form [26,27]. On the other hand, activated carbons are proven to have high porosity, good surface area, and durability. In a previous study, the powder of tamarind seeds was activated in 98% H_2SO_4 solution and employed for Methylene blue dye adsorption [28]. In a work of its first kind, commercial activated carbons composited with CHS were used for the adsorption of ibuprofen [29]. Polyvinyl alcohol (PVA) and glutaraldehyde (GTA) were used as a hydrophilic agent and crosslinking agent, respectively, in the composite preparation [29]. PVA is a nontoxic, biocompatible, and

biodegradable polymer with all desirable properties such as high physical strength, excellent film-forming ability, hydrophilicity, enhanced tensile strength [29,30]. GTA enhances the acid stability of CHS in the crosslinking and improves the mechanical properties of the composite [31–33].

In this work, the adsorption of MB and MO from their aqueous solutions on TSAC and CHS-TSAC composite was reported. PVA and GTA were utilized as a hydrophilic agent and crosslinking agent, respectively, in the preparation of the CHS-TSAC composite. In the batch adsorption experiments, the effects of pH, adsorbent dosage, initial concentration, time adsorption, and kinetics were studied. The adsorption isotherms were experimentally obtained, and regeneration of the adsorbents was reported.

2. Materials and methods

Activated carbon was prepared from tamarind seeds modified with phosphoric acid, and CHS was used to make a composite with PVA as a hydrophilic agent and GTA as a crosslinking agent. Two adsorbents, namely TSAC and CHS-TSAC, were employed for the adsorption of MO and MB from their aqueous solution.

2.1. Preparation of aqueous solution

Aqueous solutions were prepared from Milli-Q water for the batch adsorption studies. For each dye, 0.1 g of the dye was added to 1,000 mL of Milli-Q water to obtain 100 ppm of stock solutions. The solutions of different concentrations in the range of 5–50 mg/L were prepared with the appropriate dilution of the stock solution. The alteration of pH was done using 0.02 N HCl and/or 0.02 N NaOH.

2.2. Preparation of TSAC and CHS-TSAC

Raw tamarind seeds were first washed several times with Milli-Q water for the removal of dirt and then dried in an oven at 110°C overnight. The seeds were crushed and meshed to acquire a particle size <0.5 mm. Subsequently, the tamarind seed biomass was carbonized for 2 h in a muffle furnace at a temperature of 700°C. The charred product was activated with orthophosphoric acid of 85% purity, 2:1 w/w, respectively. For the removal of residual acid in the filtrate, acidic biomass was washed with Milli-Q water several times till the pH of the filtrate was 6.5 or above. Thus, the acid-treated tamarind seed carbon was dried at 110°C overnight in an oven (METTLER, England) followed by cooling at room temperature and was kept in desiccators for further use as TSAC [34].

For the preparation of CHS-TSAC bio-composite, deacetylated chitosan was dissolved in deionized water containing 2% (w/w) acetic acid for a 5% (w/v) chitosan solution, and the solution was stirred overnight. 5% (w/w) PVA aqueous solution was prepared with Milli-Q water. The solutions of CHS and PVA were mixed in 1:1 (w/w) ratio and stirred overnight at 60°C to obtain a homogenous solution. TSAC and the homogeneous solution (of CHS and PVA) were mixed 1:1 w/w, and a homogenous mixture (CHS-TSAC) was prepared. For this mixture, 50% GTA aqueous

solution was added to the mixture (2%, w/w) and stirred for a day. After this crosslinking step, the bio-composite thus prepared was washed with Milli-Q for the removal of unreacted compounds followed by drying at room temperature for 24 h [29]. The schematic reaction mechanism of the adsorbent is shown in Fig. 1.

2.3. Characterization of TSAC and CHS-TSAC composite

The morphological surface and elemental composition of the adsorbents were measured using scanning electron microscopy (SEM) with energy-dispersive X-ray (EDX) analysis. The adsorbents were tested with the X-ray diffraction (XRD) technique to ascertain the amorphous or crystalline nature. The functional groups on the surface of the adsorbents were recorded using a Fourier-transform infrared (FTIR) spectrometer (Jasco FTIR 4700) and Brunauer-Emmett-Teller (BET) surface analyzer.

2.4. Effect of pH and adsorbent dosage

In order to study the effect of pH on dye adsorption, pH values were varied from 2 to 12. The pH of the solution was adjusted with 0.02 N HCl and 0.02 N NaOH to prepare a set of aqueous solutions of dyes of pH values 2, 4, 6, 8, 10, and 12. Effect of adsorbent dosage on adsorption was tested for the solution pH value where maximum adsorption capacity was seen. The effect of adsorbent dosage was tested for five different adsorbent dosage values (1, 1.5, 2.0, 2.5 and 3.0 g/L).

2.5. Adsorption isotherms and kinetics

Using the best pH value of the solution and adsorbent dosage for maximum batch adsorption as described above, the batch adsorption experiments for the generation of adsorption isotherms were conducted for each adsorbent-dye combination by varying the initial concentrations of the dye solution (5–50 mg/L with an increment of 5 mg/L).

The adsorption capacity (q_e) was measured by Eq. (1):

$$q_e = \frac{(C_i - C_e)V}{1,000W} \quad (1)$$

where C_i and C_e are initial and equilibrium concentration of dye in mg/L, W is the dosage of the adsorbent (mg), and V is the volume of the solution (mL).

For a given adsorbent-dye combination, the kinetics of the adsorption was studied for the best pH value, adsorbent dosage, and initial concentration of the dye at room temperature. The samples of dye solutions from the rotating flask of batch adsorption experiments were collected periodically for testing.

2.6. Regeneration study

In order to separate the dye adhered to the adsorbents, the loaded adsorbents were washed several times with Milli-Q water followed by drying at 60°C for 12 h in an oven. Then, the adsorbent is added to 10 mL of 0.1 M HCl solution and stirred for 24 h. After filtration, the adsorbents

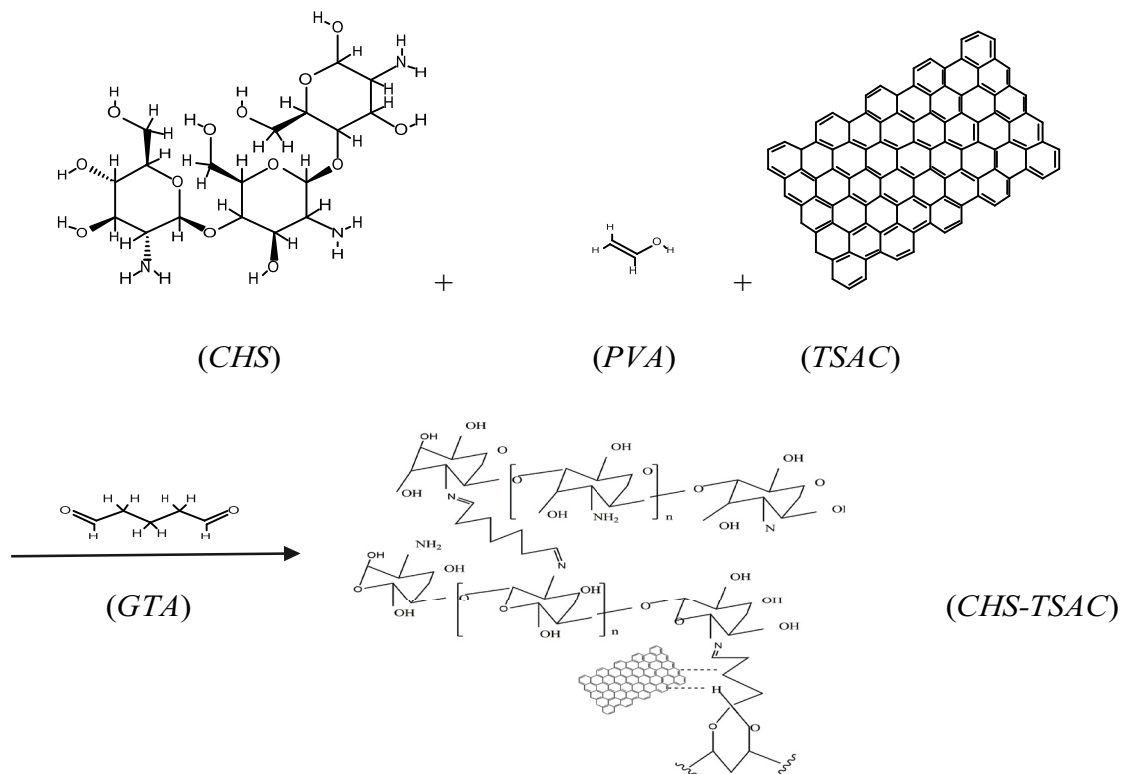


Fig. 1. Preparation of CHS-TSAC, reaction mechanism.

were dried at 45°C for 12 h and used for the subsequent adsorption experiments [35].

3. Results and discussion

3.1. Characterizations

3.1.1. Scanning electron microscopy and energy-dispersive X-ray spectroscopy

The surfaces of TSAC and CHS-TSAC were irregular, heterogeneous, and rough with cavities in all cases. However, the surface of TSAC was more porous. The surface patterning in the case of CHS-TSAC is quite different from that of TSAC. It could be attributed to the crosslinking of the activated carbon with chitosan [29,36]. In order to know the compositional elements of the adsorbents, EDX was performed. There was a reduction in the carbon content and an increase in the proportions of the other elements in the case of CHS-TSAC composite due to the presence of PVA and GTA.

3.1.2. X-ray diffraction

The adsorbents were tested for their crystallinity nature using the X-ray diffraction technique. The two adsorbents were predominantly amorphous in nature, as two broad peaks were observed at 20° and 42° [37]. The peak corresponding to the plane (100) corresponds to the micrographical phase, which is typical of carbonaceous materials [38]. The peak of (002) of CHS-TSAC was slightly broader due to the presence of oxygen-containing groups contributed by the presence of CHS [24].

3.1.3. Fourier-transform infrared spectroscopy

In order to study the presence and nature of the various functional groups on the surface of the adsorbents, FTIR analysis was carried out for both the adsorbents, and the results are shown in Fig. 2. For both TSAC and CHS-TSAC, the common bonds observed were P=O (1,150 cm⁻¹), epoxy stretching vibrations C–O (1,270 cm⁻¹), medium intensity C–H

(1,567 cm⁻¹), alkyne medium strength bond C≡C (2,050 cm⁻¹), and OH (3,402 cm⁻¹). Few additional bonds were visible in the CHS-TSAC composite, which were moderately intensive such as C–N (1,030 cm⁻¹) and N–H (3,201 cm⁻¹), indicating the presence of chitosan. It can be seen from Fig. 2 that the medium bands between 1,000–1,300 cm⁻¹ were due to H₃PO₄ activation. The peak at 1,150 cm⁻¹ corresponds to the stretching vibrations of P=O, stretching of O–C in P–O–C linkage, and P=OOH [39]. The stretching vibration of C–N (1,030 cm⁻¹) and bending vibration N–H (3,201 cm⁻¹) prove the successful synthesis of the composite.

3.1.4. Brunauer–Emmett–Teller

BET surface area measurement is a standard method to measure the specific surface area and pore size distribution based on nitrogen adsorption–desorption isotherm. As shown in Fig. 3, the obtained isotherm indicates a macroporous nature for both the adsorbents as the mean pore diameters were greater than 50 nm (TSAC – 53.674 nm; TSAC-CHS – 53.192 nm). For both the materials, at the lower pressures, very little adsorption of nitrogen was seen. A sudden increase in the adsorption capacity was seen at a relative pressure of 0.9 for both adsorbents. For TSAC (TSAC-CHS), the mean volume and specific surface area obtained were 0.3139 (0.2112) cm³/g and 1.3665 (0.91912) m²/g, respectively.

3.2. Adsorption estimation

3.2.1. Effect of pH and adsorbent dosage on MB and MO adsorption

The batch adsorption studies for the selection of optimal pH were performed in a shaking incubator (Labline, ISO certified – 9001-2008) with conical flasks for 2 h time at 100 rpm and room temperature. An adsorbent dosage of 4 g/L was added to the 50 mL dye solution of 40 mg/L in the conical flasks for this purpose. After batch adsorption, the concentration of the dye in the solution was measured using a UV spectrophotometer (λ , PerkinElmer). For MB and MO, the absorbance values are 664 and 464 nm, respectively. The effect of pH on the adsorption of MB

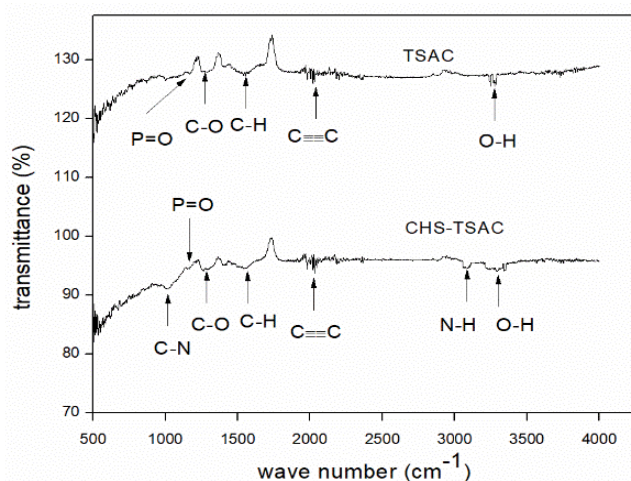


Fig. 2. FTIR analysis.

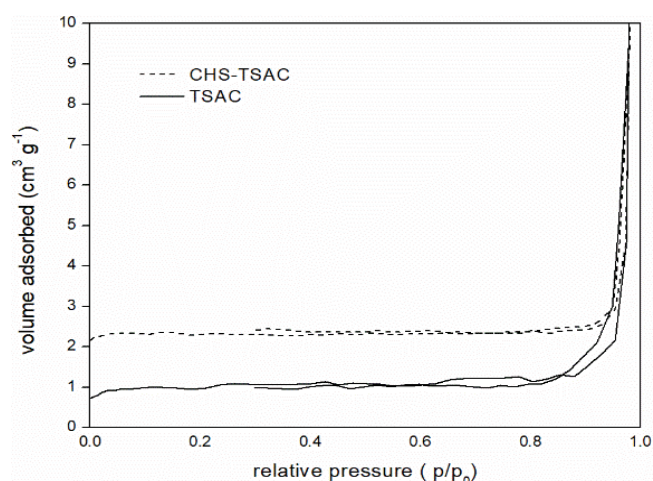


Fig. 3. Nitrogen adsorption–desorption for the adsorbents.

and MO onto the TSAC and CHS-TSAC was studied in the range of 2–12 (± 0.05) and shown in Fig. 4a. The presence of H^+ or OH^- in excess is one of the key factors affecting the organic dye ions adsorption ensuing protonation/deprotonation of the adsorbent's functional groups [40,41]. The optimum adsorption capacities for MB and MO were obtained at pH values of 10 and 3 respectively for the adsorbent dosage of 10 mg/L for both TSAC and CHS-TSAC. The adsorbent surface acquires an overall positive charge at lower pH values, thus attracting the anionic dye MO due to electrostatic interactions. On the other hand, higher pH values of the solution result in the effective adsorption of cationic MB. It is due to the strong electrostatic interactions between the positively imposed cationic MB dye and the overall negative charge of the adsorbent surface at the higher pH values of the solution. In comparison, CHS-TSAC exhibited better adsorption characteristics for MO. Nevertheless, for MB, both adsorbents showed an almost similar trend for the adsorption of MB with respect to pH.

Fig. 4b depicts the effect of adsorbent dosage on MB and MO adsorption amount in the range of 10 mg to 30 mg in 50 mL solution with 40 mg/L dye concentration at the respective optimal values of pH. It can be seen that the adsorption capacity decreases with increasing adsorbent dose. The active sites on the surface may get saturated when the dosage amount increases [42,43], or the higher adsorbent dosages cause agglomeration of the adsorbent particles leading to blockage of the active sites thus lowering the adsorption capacity upon the further increase in the adsorbent dosage amount.

3.2.2. Effect of initial concentration and nonlinear equilibrium studies on MB and MO adsorption

The effect of initial concentration on the adsorption amount and percentage removal is shown in Figs. 5a and b. These experiments were performed at the respective optimal pH values and 10 mg of adsorbent dosage per 50 mL of solution. For TSAC, the maximum adsorption capacity values are 142.12 mg/g (MB) and 71.8 mg/g (MO) at

40 mg/L of the initial concentration of the dye. In the case of CHS-TSAC, the maximum adsorption capacity value is 140.62 mg/g for MB at 40 mg/L of the initial concentration of the dye. The maximum adsorption capacity for MO using CHS-TSAC is 94.45 mg/g at 50 mg/L of the initial concentration of the dye. The composite exhibited superior adsorption characteristics for the removal of MO, possibly due to the presence of positively charged amino groups.

For TSAC, the maximum percentage removal values are 71.06 (MB) and 36.6 (MO). On the other hand, the values are 70.3 (MB) and 37.7 (MO) in the case of CHS-TSAC. The equilibrium data of each adsorbent-dye combination were fitted to four nonlinear adsorption isotherm models, namely Langmuir, Freundlich, Temkin, and Dubinin-Radushkevich (D-R). The details of these models are shown in Table 1, while the values of the parameters of the models after fitting the adsorption data are tabulated in Table 2. The experimental and theoretical adsorption capacity values at different equilibrium concentrations are plotted in Fig. 6. The curves depict the equilibrium adsorption behavior of the dyes on the two adsorbents. From the plots, it can be seen that the Langmuir adsorption isotherm model was best suitable to depict the adsorption of MB and MO on the two adsorbents. Moreover, as shown in Table 2, the equilibrium adsorption data of both TSAC and CHS-TSAC composite were best fitted to the Langmuir model with the highest R^2 values. The values of n for the Freundlich adsorption model are greater than one in all four cases and hence unfavorable [44]. For the Temkin isotherm model, the values of B for the adsorption of MB and MO on CHS-TSAC are 30.8 and 24.10 J/mol, respectively. It indicates that the adsorption of ions was very strong as the values of B are greater than 20 J/mol [45]. Finally, the mean free energy was computed using the formula $E_D = 1/\sqrt{2K_{DR}}$. The significance of mean free energy in D-R isotherm model is to compare the chemisorption and physisorption [20]. Since the value of E_D are less than 8 kJ/mol in all the cases, it indicates that the adsorption behavior is majorly physisorption type. Note that the fitting of the data using D-R isotherm model is not satisfactory as the R^2 values are quite away from unity.

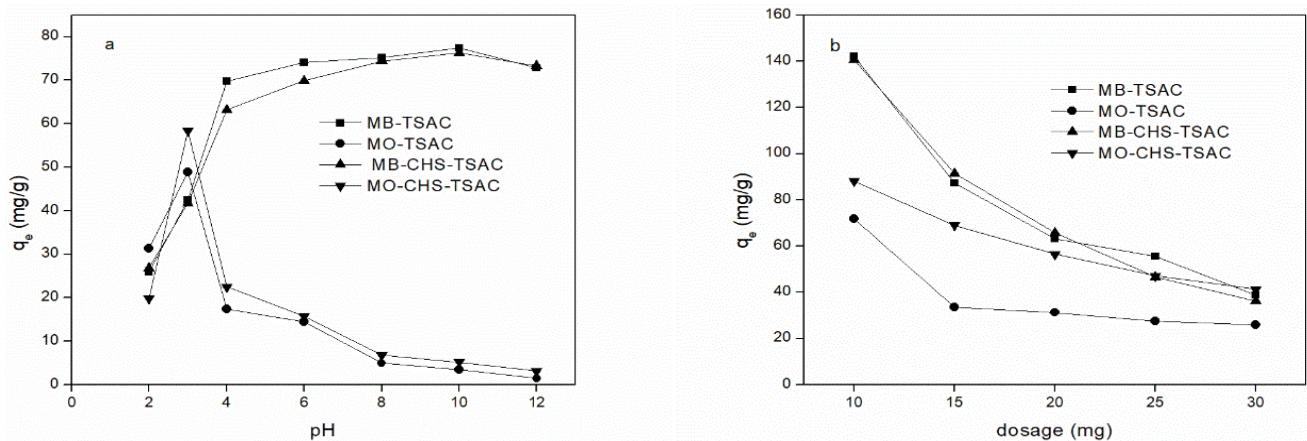


Fig. 4. MB and MO adsorption (a) effect of initial pH at room temperature (initial concentration of both the dyes = 40 ppm, the dosage of both the adsorbents = 20 mg/50 mL, contact time = 2 h and (b) effect of adsorbent dosage at room temperature (pH = 10 for MB and 3 for MO, initial concentration of both the dyes = 40 ppm, contact time = 2 h).

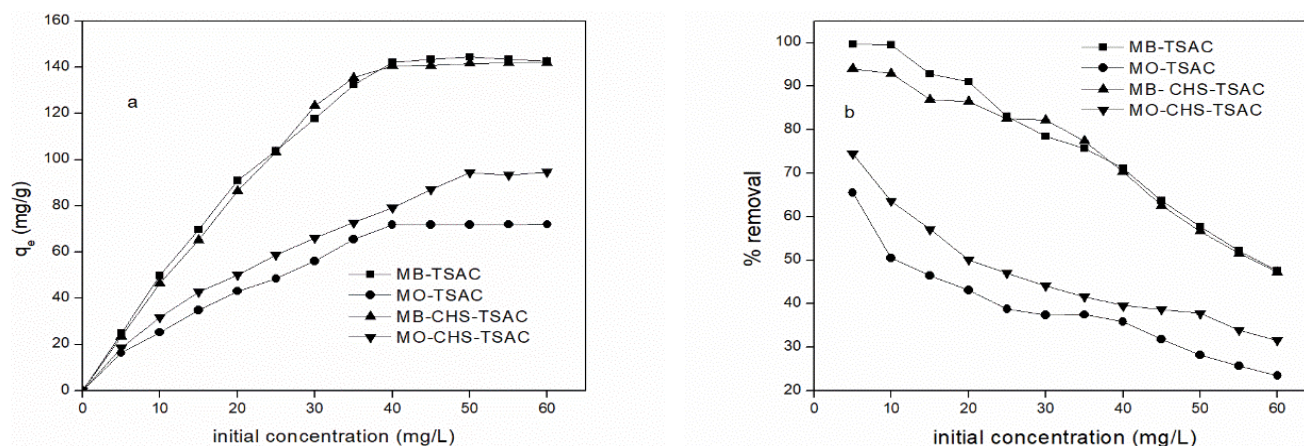


Fig. 5. Effect of initial concentration on MB and MO adsorption at room temperature (pH = 10 for MB and 3 for MO, dosage of both the adsorbents = 10 mg/50 mL, contact time = 2 h (a) adsorption amount and (b) % removal.

Table 1
Adsorption equilibrium models

Model name	Nonlinear model equation	Variables
Langmuir	$q_e = \frac{K_L q_m C_e}{(1 + K_L C_e)}$	C_e = Equilibrium concentration of adsorbate (mg/L); K_L = Langmuir isotherm constant (L/mg); q_e = Number of dye adsorbed per unit gram of the adsorbent at equilibrium (mg/g); q_m = Maximum adsorption capacity (mg/g).
Freundlich	$q_e = K_f C_e^{1/n}$	n = Adsorption intensity; K_f = Freundlich isotherm constant (mg/g).
Temkin	$q_e = \frac{RT}{b_T} \ln(A_T C_e)$	A_T = Temkin isotherm equilibrium binding constant (L/g); R = Universal gas constant (8.314 J/mol/K); b_T = Temkin isotherm constant kJ/mol; T = Temperature at 300.15 K.
D-R	$q_e = q_s \exp(-K_{DR} E_D^2)$	K_{DR} = Dubinin–Radushkevich isotherm constant (mol ² /kJ ²); q_s = Theoretical isotherm saturation capacity (mg/g); E_D = mean free energy kJ/mol.

Table 2
Parameter values of the four adsorption isotherms

Model	Adsorbent	Parameters for MB			Parameters for MO		
Langmuir	TSAC	$q_e = 149.55$	$K_L = 0.82744$	$R^2 = 0.9818$	$q_m = 107.78$	$K_L = 0.0621$	$R^2 = 0.9780$
	CHS-TSAC	$q_e = 146.417$	$K_L = 0.45421$	$R^2 = 0.9823$	$q_m = 127.75$	$K_L = 0.0719$	$R^2 = 0.9815$
Freundlich	TSAC	$K_f = 78.344$	$n = 4.5669$	$R^2 = 0.9807$	$K_f = 12.479$	$n = 1.959$	$R^2 = 0.9751$
	CHS-TSAC	$K_f = 61.32$	$n = 3.2024$	$R^2 = 0.9248$	$K_f = 17.79$	$n = 2.145$	$R^2 = 0.961$
Temkin	TSAC	$A_T = 241$	$b_T = 151.6$	$R^2 = 0.9550$	$A_T = 0.872$	$b_T = 120.297$	$R^2 = 0.9523$
	CHS-TSAC	$A_T = 6.62$	$b_T = 80.97$	$R^2 = 0.9681$	$A_T = 1.12$	$b_T = 103.4$	$R^2 = 0.9636$
D-R	TSAC	$q_s = 112.5$	$K_{DR} = 1.36 \times 10^{-8}$	$R^2 = 0.8387$	$q_s = 52.51$	$K_{DR} = 9.76 \times 10^{-7}$	$R^2 = 0.6685$
	CHS-TSAC	$q_s = 112.1$	$E_D = 6.056$	$R^2 = 0.8277$	$q_s = 61.99$	$E_D = 0.715$	$R^2 = 0.6902$
			$E_D = 1.98$			$K_{DR} = 6.24 \times 10^{-7}$	$R^2 = 0.6902$
						$E_D = 0.895$	

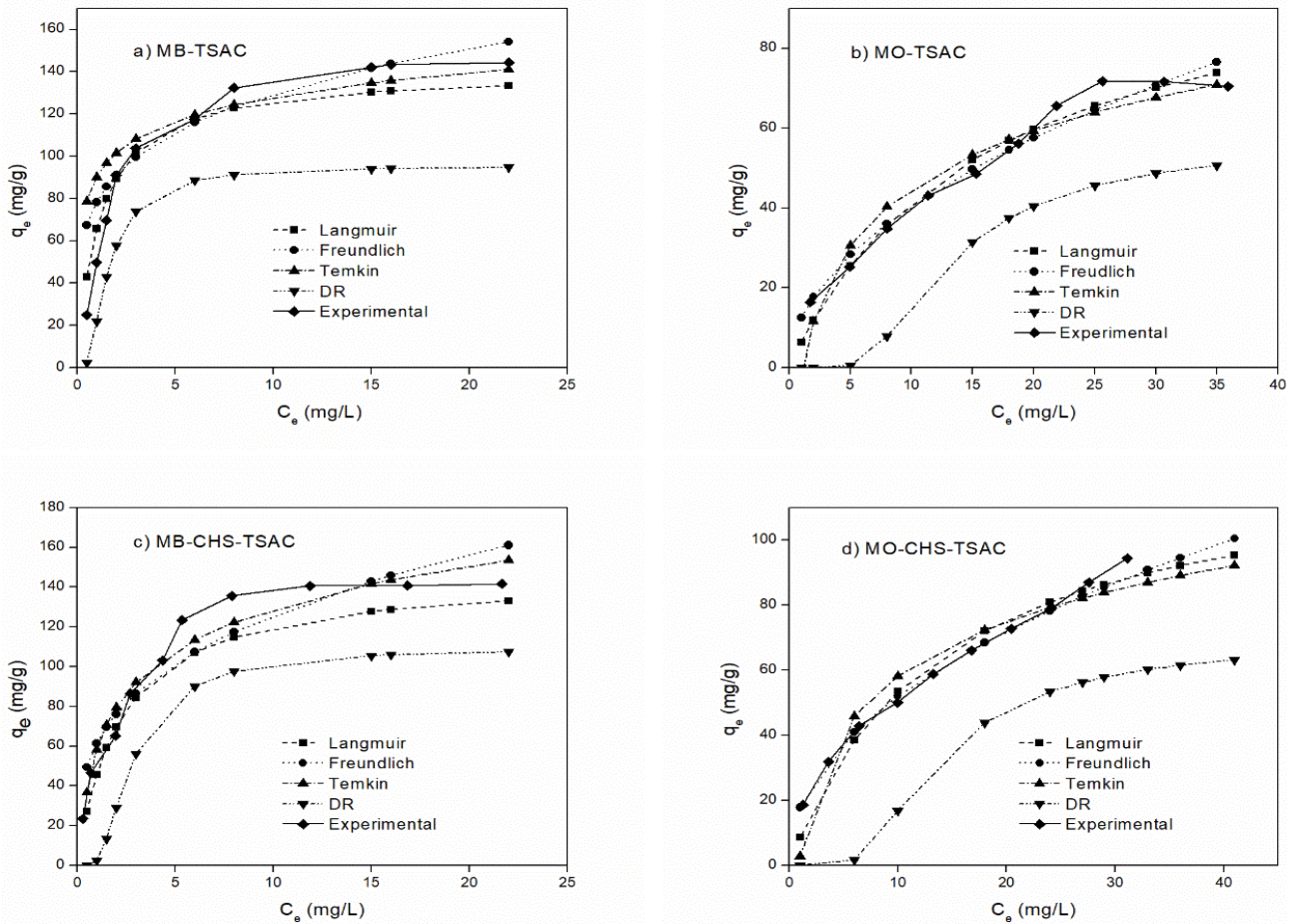


Fig. 6. The equilibrium adsorption curves of four nonlinear isotherm models, (a) MB-TSAC, (b) MO-TSAC and (c) MB-CHS-TSAC, and (d) MO-CHS-TSAC.

3.2.3. Kinetic studies

Fig. 7 shows adsorption of MB and MO on TSAC and CHS-TSAC with respect to time at room temperature (pH values of 10 and 3 for MB and MO solutions respectively) with 40 mg/L of an aqueous solution except CHS-TSAC and MO combination where 50 mg/L was the initial concentration of the solution. It was found that equilibrium adsorption capacity was attained at 100 min of contact time for the two adsorbents. Table 3 shows two kinetic models (pseudo-first-order, pseudo-second-order) and the parameters of the models after fitting the data. The experimental data along with the calculated values from the model equations, are plotted in Figs. 8a–d. For the equations shown in Table 3, q_t and q_e are the amounts of adsorbate per mass of adsorbent (mg/g) at any time and equilibrium, respectively. All the adsorbents exhibited the most significant degree of correlation to the pseudo-second-order nonlinear model kinetics compared to the other kinetic models. The kinetics were best fitted to the pseudo-second-order model, and the rate constants were 0.00134 and 0.00136 g/mg min for the sorption of MB, and 0.0005 and 0.00085 g/mg min for MO sorption, for TSAC and CHS-TSAC, respectively.

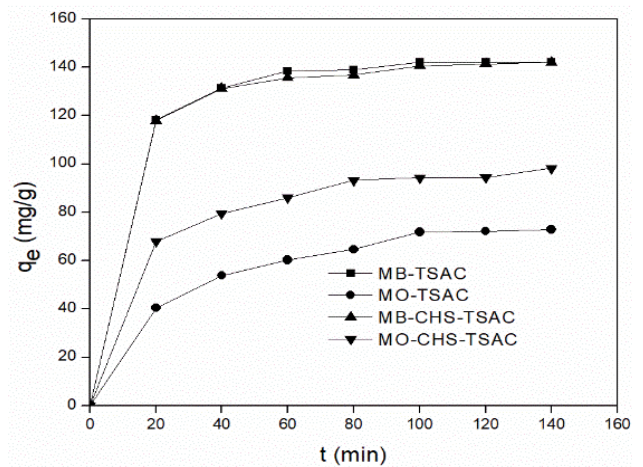


Fig. 7. Effect of time on MB and MO adsorption at room temperature (pH = 10 for MB and 3 for MO, adsorbent dosage of both the adsorbents = 10 mg/50 mL, contact time 2 h).

Table 3
Calculated parameter values of two kinetic models

Kinetic model	Equation	Adsorbent	Parameters for MB						Parameters for MO		
			K_1 (min ⁻¹), K_2 (g mg ⁻¹ min ⁻¹) and q_e (mg/g)								
Pseudo-first-order	$q_t = q_e(1 - e^{-K_1 t})$	TSAC	$K_1 = 26.23$	$q_e = 136.2$	$R^2 = 0.9675$	$K_1 = 12.56$	$q_e = 62.3$	$R^2 = 0.7647$			
		CHS-TSAC	$K_1 = 26.17$	$q_e = 135.5$	$R^2 = 0.9683$	$K_1 = 17.051$	$q_e = 87.65$	$R^2 = 0.891$			
Pseudo-second-order	$q_t = \frac{tK_2 q_e^2}{1 + K_2 t q_e}$	TSAC	$K_2 = 0.00134$	$q_e = 148.3$	$R^2 = 0.9995$	$K_2 = 0.0005$	$q_e = 85.56$	$R^2 = 0.9967$			
		CHS-TSAC	$K_2 = 0.00136$	$q_e = 147.5$	$R^2 = 0.9998$	$K_2 = 0.00085$	$q_e = 104.8$	$R^2 = 0.9976$			

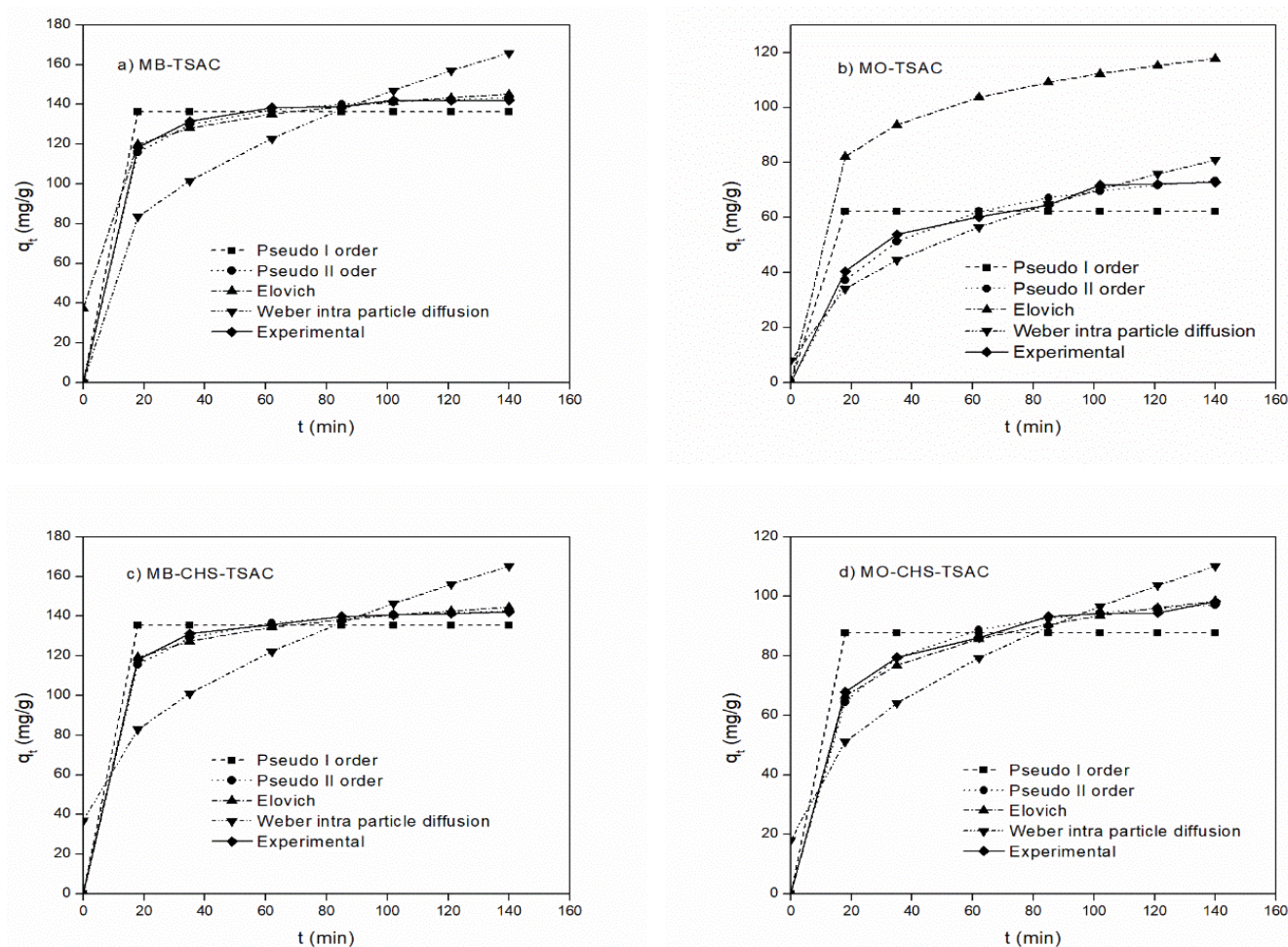


Fig. 8. Four nonlinear kinetic models, (a) MB-TSAC, (b) MO-TSAC and (c) MB-CHS-TSAC, and (d) MO-CHS-TSAC.

4. Adsorption mechanism

4.1. Electrostatic interactions

As per the optimal pH values for the maximum adsorption, the adsorption mechanism of the dyes on the two adsorbents is chiefly attributed to electrostatic interactions. The point of zero charges (PZC) is shown in Fig. 9. The PZC for both adsorbents was found to be equal 6.93 approximately. For the CHS-TSAC, the optimal pH values for the maximum adsorption for MB and MO are 10 and 3, respectively. The electrostatic interactions between

cationic MB dye and anionic PO_4^- groups of the adsorbents are enhanced with the increase of pH values and attained maximum at a pH value of 10, as shown in Fig. 4a. Since MO is an anionic dye, at a pH value of 3 for the solution, both adsorbents exhibited almost similar adsorption capacity characteristics, as shown in Fig. 4. However, CHS-TSAC yielded to higher values of adsorption capacity at pH values greater than 3. The interaction between SO_3^- of MO dye and the positively charged amino groups of the composite and the bonding between H^+ on the adsorbent surface with O and N of the MO dye could be

a reason for this trend [35,46,47]. The adsorption capacity values performance is more for MB because the molecular weight of MB is lesser as compared to MO [48].

4.2. Weber’s intraparticle diffusion model

Weber’s intraparticle diffusion model describes the mechanism of adsorption. The model equation and the constants of the model for each pair are shown in Table 4. Also, the experimental data are plotted in Fig. 10 as per Weber’s model equation. The adsorption phases were divided into three regions in the figure. In the region I, the adsorption of MB appears to be rapid. On the other hand, the adsorption of MO is slower or not so rapid. The intercept values obtained after fitting the data to this model indicate that the boundary layer is thick in the case of MB adsorption on these adsorbents. The values of the intercept (C) were greater for MB showing the highly effective boundary layer for mass transfer for MB as compared to MO. The curves in the region II are linear, indicating intraparticle diffusion in the adsorption for all four cases. However, the curves do not pass through the origin in the case of MB, suggesting rate-controlling steps other than intraparticle diffusion in the adsorption of MB on these two adsorbents. Intraparticle diffusion is the main rate-controlling step in the case of MO since the curves of MO in the region II appear to intercept the y-axis near the origin [49].

4.3. Elovich model

Elovich nonlinear model equation is shown in Table 4, and it describes chemisorption. The number of sites available

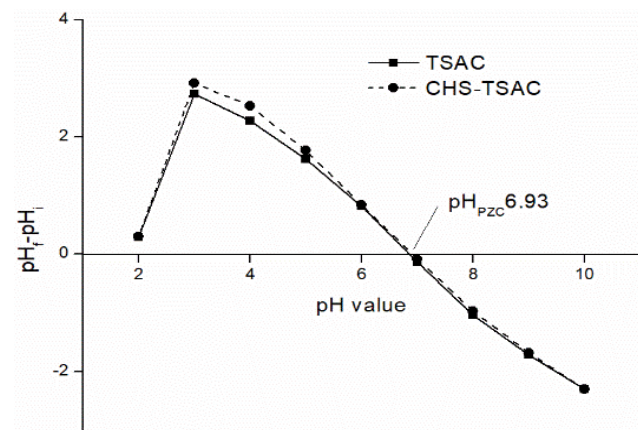


Fig. 9. Point of zero charges of TSAC and CHS-TSAC.

for the adsorption is known from the value of $1/\beta$ and $1/\beta \ln(\alpha\beta)$ represents the quantity of adsorption when $\ln t = 0$ [50,51]. As the amount of adsorbed molecules increases, the biosorption rate decreases exponentially as per the model. The R^2 values are very close to unity in all the cases. This trend indicates the chemisorption nature of the adsorption. For the equations tabulated in Table 4, q_t and q_e are the amount of metal adsorbed per mass of adsorbent (mg/g) at any time and equilibrium, respectively, K_{id} = intraparticle diffusion rate constant (mg/g min^{0.5}), β is initial adsorption rate (mg/g min), and a is desorption constant (mg/g min).

4.4. Comparison with previous similar studies

The maximum adsorption capacity values for MB and MO removal using several adsorbents reported in the literature are presented in Table 5. For MB removal, the activated carbon and the composite synthesized in the current study exhibited superior adsorption capacity except polyvinyl alcohol/carboxymethyl cellulose hydrogels reinforced with graphene oxide and bentonite [53]. The table shows that the adsorption capacity of the composite CHS-TSAC is highest among the tabulated ones for adsorptive removal of MO.

5. Regeneration study

For large-scale operations, recovery of the adsorbent should be considered as a significant step. The reusability

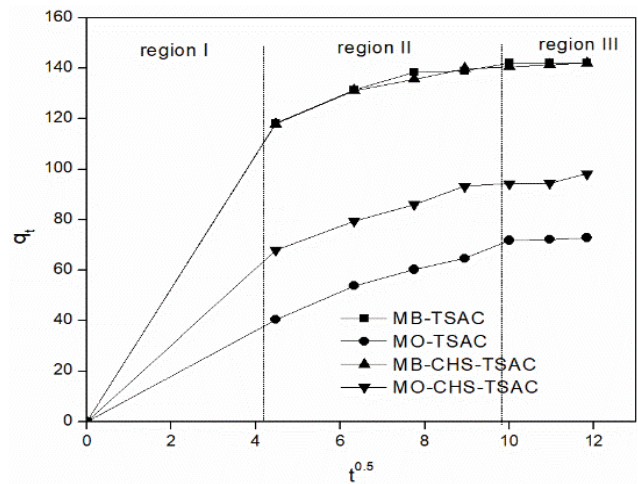


Fig. 10. Weber intraparticle diffusion model.

Table 4
Calculated parameter values of two nonlinear diffusion models

Kinetic model	Equation	Adsorbent	Parameters for MB			Parameters for MO		
			K_{id} (mg/g min ^{0.5})	β (mg/g min)	a (mg/g min)	K_{id} (mg/g min ^{0.5})	c	R^2
Weber intraparticle diffusion	$q_t = K_{id}t^{0.5} + C$	TSAC	$K_{id} = 10.87$	$C = 37.23$	$R^2 = 0.71$	$K_{id} = 6.155$	$c = 8.115$	$R^2 = 0.9238$
		CHS-TSAC	$K_{id} = 10.83$	$C = 36.98$	$R^2 = 0.7107$	$K_{id} = 7.776$	$c = 18.12$	$R^2 = 0.8405$
Elovich model	$q_t = \frac{1}{\beta} \ln(\alpha\beta t)$	TSAC	$\beta = 0.0812$	$a = 11568$	$R^2 = 0.9973$	$\beta = 0.058$	$a = 9.336$	$R^2 = 0.996$
		CHS-TSAC	$\beta = 0.08153$	$a = 11421$	$R^2 = 0.998$	$\beta = 0.0644$	$a = 65.055$	$R^2 = 0.997$

Table 5
Adsorption capacities obtained in the previous study

S. No.	Adsorbate	Adsorbent	Adsorption capacity (mg/g)	Reference
1	MB	Raw and surface modified tamarind with H ₂ SO ₄	16.611 and 34.483	[28]
2	MB	Core shell structures polystyrene@graphene oxide composite	59.07	[52]
3	MB	Activated carbon prepared from waste tire	1.05	[12]
4	MB	Polyvinyl alcohol/carboxymethyl cellulose hydrogels reinforced with graphene oxide and bentonite	172.14	[53]
5	MB	TSAC and CHS-TSAC	142.12 and 140.62, respectively	Present study
6	MO	Chitosan graphene oxide composite aerogel	48.6	[54]
7	MO	Bottom ash and de-oiled soya	3.618 and 16.664	[11]
8	MO	MnFe ₂ O ₄ -chitosan modified biochar	90.35	[1]
9	MO	TSAC and CHS-TSAC	71.8 and 94.45, respectively	Present study

of TSAC and CHS-TSAC was studied as the regeneration studies using 0.1 M HCl for three adsorption–desorption cycles. In the desorption studies, both the adsorbents were successfully regenerated. For the third cycle, the adsorption capacity with TSAC was 138.35 and 69.2 mg/g for MB and MO, respectively. The adsorption capacity of the adsorbents slightly decreased over the cycles in the case of CHS-TSAC. Overall, this study establishes the application of the adsorbents at the industrial level for the removal of MB and MO from wastewater.

6. Conclusion

In this research work, two adsorbents, namely TSAC and CHS-TSAC were synthesized and tested for the removal of two commonly used dyes, namely Methylene blue (MB) and Methyl orange (MO). TSAC is an activated carbon synthesized using tamarind seeds, while CHS-TSAC is a composite made by the combination of chitosan and TSAC. For batch adsorption, the optimal values of pH, adsorbent dosage, and initial concentration, and adsorption time were experimentally determined. At the respective optimal conditions, the maximum adsorption capacity values of the adsorbents for MB were almost the same, while CHS-TSAC exhibited a higher maximum adsorption capacity for MO. The characterization of the adsorbents revealed the presence of various functional groups which can aid the adsorption process. More importantly, the batch equilibrium adsorption data was experimentally obtained and fitted to four isotherm models in their nonlinear forms. The adsorption, in all cases, was best represented by the Langmuir adsorption isotherm model, and the adsorption kinetics followed the pseudo-second-order kinetic model. The adsorption of MB was favourable at higher pH values. Since MB is a cationic dye, it is evident that the cationic form of dye can be held by the adsorbent surface, whose overall charge becomes negative at the higher pH values. On the other hand, at a pH of 3, the adsorption of anionic MO on both adsorbents was maximum. The MB adsorption was rapid to that of MO. The successful regeneration studies suggest the suitability of the adsorbents in the water treatment industry.

References

- [1] Z. Wang, Y. Li, X. Xie, Z. Wang, Bifunctional MnFe₂O₄/chitosan modified biochar composite for enhanced Methyl orange removal based on adsorption and photo-Fenton process, *Colloids Surf., A*, 613 (2021) 126104, doi: 10.1016/j.colsurfa.2020.126104.
- [2] H. Yang, H. Yuan, Q. Hu, W. Liu, D. Zhang, Synthesis of mesoporous C/MoS₂ for adsorption of Methyl orange and photo-catalytic sterilization, *Appl. Surf. Sci.*, 504 (2020) 144445, doi: 10.1016/j.apsusc.2019.144445.
- [3] A. Ajmal, I. Majeed, R.N. Malik, H. Idriss, M.A. Nadeem, Principles and mechanisms of photocatalytic dye degradation on TiO₂ based photocatalysts: a comparative overview, *RSC Adv.*, 4 (2014) 37003–37026.
- [4] H.P. Mota, R.F.N. Quadrado, T.A.L. Burgo, B.A. Iglesias, A.R. Fajardo, Polysaccharide/Fe(III)-porphyrin hybrid film as catalyst for oxidative decolorization of toxic azo dyes: an approach for wastewater treatment, *Arabian J. Chem.*, 13 (2020) 5923–5938.
- [5] A.K. Prajapati, M.K. Mondal, Comprehensive kinetic and mass transfer modeling for Methylene blue dye adsorption onto CuO nanoparticles loaded on nanoporous activated carbon prepared from waste coconut shell, *J. Mol. Liq.*, 307 (2020) 112949, doi: 10.1016/j.molliq.2020.112949.
- [6] T. Rasheed, M. Bilal, F. Nabeel, M. Adeel, H.M.N. Iqbal, Environmentally-related contaminants of high concern: potential sources and analytical modalities for detection, quantification, and treatment, *Environ. Int.*, 122 (2019) 52–66.
- [7] K. Shahul Hameed, P. Muthirulan, M. Meenakshi Sundaram, Adsorption of chromotrope dye onto activated carbons obtained from the seeds of various plants: equilibrium and kinetics studies, *Arabian J. Chem.*, 10 (2017) S2225–S2233.
- [8] J. Mittal, A. Mariyam, F. Sakina, R.T. Baker, A.K. Sharma, A. Mittal, Batch and bulk adsorptive removal of anionic dye using metal/halide-free ordered mesoporous carbon as adsorbent, *J. Cleaner Prod.*, 321 (2021) 129060, doi: 10.1016/j.jclepro.2021.129060.
- [9] M. Landarani, M. Arab Chamjangali, B. Bahramian, Preparation and characterization of a novel chemically modified PVC adsorbent for Methyl orange removal: optimization, and study of isotherm, kinetics, and thermodynamics of adsorption process, *Water Air Soil Pollut.*, 231 (2020) 513, doi: 10.1007/s11270-020-04874-7.
- [10] W. Deligeer, Y.W. Gao, S. Asuha, Adsorption of Methyl orange on mesoporous γ -Fe₂O₃/SiO₂ nanocomposites, *Appl. Surf. Sci.*, 257 (2011) 3524–3528.
- [11] A. Mittal, A. Malviya, D. Kaur, J. Mittal, L. Kurup, Studies on the adsorption kinetics and isotherms for the removal and recovery of Methyl orange from wastewaters using waste materials, *J. Hazard. Mater.*, 148 (2007) 229–240.

- [12] H. Daraei, A. Mittal, Investigation of adsorption performance of activated carbon prepared from waste tire for the removal of Methylene blue dye from wastewater, *Desal. Water Treat.*, 90 (2017) 294–298.
- [13] C. Arora, S. Soni, S. Sahu, J. Mittal, P. Kumar, P.K. Bajpai, Iron based metal organic framework for efficient removal of Methylene blue dye from industrial waste, *J. Mol. Liq.*, 284 (2019) 343–352.
- [14] B. Chen, H. Zhao, S. Chen, F. Long, B. Huang, B. Yang, X. Pan, A magnetically recyclable chitosan composite adsorbent functionalized with EDTA for simultaneous capture of anionic dye and heavy metals in complex wastewater, *Chem. Eng. J.*, 356 (2019) 69–80.
- [15] A. Mariyam, J. Mittal, F. Sakina, R.T. Baker, A.K. Sharma, A. Mittal, Efficient batch and fixed-bed sequestration of a basic dye using a novel variant of ordered mesoporous carbon as adsorbent, *Arabian J. Chem.*, 14 (2021) 103186, doi: 10.1016/j.arabj.2021.103186.
- [16] I. Anastopoulos, I. Pashalidis, A.G. Orfanos, I.D. Manariotis, T. Tatarchuk, L. Sellaoui, A. Bonilla-Petriciolet, A. Mittal, A. Núñez-Delgado, Removal of caffeine, nicotine and amoxicillin from (waste)waters by various adsorbents. A review, 261 (2020) 110236, doi: 10.1016/j.jenvman.2020.110236.
- [17] J. Mittal, R. Ahmad, M.O. Ejaz, A. Mariyam, A. Mittal, A novel, eco-friendly bio-nanocomposite (Alg-Cst/Kal) for the adsorptive removal of crystal violet dye from its aqueous solutions, *Int. J. Phytorem.*, 24 (2021) 1–12, doi: 10.1080/15226514.2021.1977778.
- [18] S. Soni, P.K. Bajpai, D. Bharti, J. Mittal, C. Arora, Removal of crystal violet from aqueous solution using iron based metal organic framework, *Desal. Water Treat.*, 205 (2020) 386–399.
- [19] A. Mariyam, J. Mittal, F. Sakina, R.T. Baker, A.K. Sharma, Fixed-bed adsorption of the dye chrysoidine R on ordered mesoporous carbon, *Desal. Water Treat.*, 229 (2021) 395–402.
- [20] A. Mariyam, J. Mittal, F. Sakina, R.T. Baker, A.K. Sharma, Adsorption behaviour of Chrysoidine R dye on a metal/halide-free variant of ordered mesoporous carbon, *Desal. Water Treat.*, 223 (2021) 425–433.
- [21] J. Mittal, Recent progress in the synthesis of layered double hydroxides and their application for the adsorptive removal of dyes: a review, *J. Environ. Manage.*, 295 (2021) 113017, doi: 10.1016/j.jenvman.2021.113017.
- [22] C. Arora, P. Kumar, S. Soni, J. Mittal, A. Mittal, B. Singh, Efficient removal of malachite green dye from aqueous solution using *Curcuma caesia* based activated carbon, *Desal. Water Treat.*, 195 (2020) 341–352.
- [23] P. Saharan, V. Kumar, J. Mittal, V. Sharma, A.K. Sharma, Efficient ultrasonic assisted adsorption of organic pollutants employing bimetallic-carbon nanocomposites, *Sep. Sci. Technol.*, 56 (2021) 2895–2908.
- [24] A.H. Jawad, A.S. Abdulhameed, M.S. Mastuli, Mesoporous crosslinked chitosan-activated charcoal composite for the removal of thionine cationic dye: comprehensive adsorption and mechanism study, *J. Polym. Environ.*, 28 (2020) 1095–1105.
- [25] A.H. Jawad, M.A. Nawari, M.H. Mohamed, L.D. Wilson, Oxidation of chitosan in solution by photocatalysis and product characterization, *J. Polym. Environ.*, 25 (2017) 828–835.
- [26] A.S. Abdulhameed, A.K.-T. Mohammad, A.H. Jawad, Modeling and mechanism of reactive orange 16 dye adsorption by chitosan-glyoxal/TiO₂ nanocomposite: application of response surface methodology, *Desal. Water Treat.*, 164 (2019) 346–360.
- [27] M.A. Nawari, A.H. Jawad, S. Sabar, W.S. Wan Ngah, Photocatalytic-oxidation of solid state chitosan by immobilized bilayer assembly of TiO₂-chitosan under a compact household fluorescent lamp irradiation, *Carbohydr. Polym.*, 83 (2011) 1146–1152.
- [28] P. Senthil Kumar, R. Sivaranejee, U. Vinothini, M. Raghavi, K. Rajasekar, K. Ramakrishnan, Adsorption of dye onto raw and surface modified tamarind seeds: isotherms, process design, kinetics and mechanism, *Desal. Water Treat.*, 52 (2014) 2620–2633.
- [29] O.I. Sahin, B. Saygi-Yalcin, D. Saloglu, Adsorption of ibuprofen from wastewater using activated carbon and graphene oxide embedded chitosan-PVA: equilibrium, kinetics, and thermodynamics and optimization with central composite design, *Desal. Water Treat.*, 179 (2020) 396–417.
- [30] T. Anitha, P. Senthil Kumar, K. Sathish Kumar, K. Sriram, J. Feroze Ahmed, Biosorption of lead(II) ions onto nano-sized chitosan particle blended polyvinyl alcohol (PVA): adsorption isotherms, kinetics and equilibrium studies, *Desal. Water Treat.*, 57 (2016) 13711–13721.
- [31] A. Maleki, E. Pajootan, B. Hayati, Ethyl acrylate grafted chitosan for heavy metal removal from wastewater: equilibrium, kinetic and thermodynamic studies, *J. Taiwan Inst. Chem. Eng.*, 51 (2015) 127–134.
- [32] M.-S. Chiou, P.-Y. Ho, H.-Y. Li, Adsorption of anionic dyes in acid solutions using chemically cross-linked chitosan beads, *Dyes Pigm.*, 60 (2004) 69–84.
- [33] N. Salehi, A. Moghimi, H. Shahbazi, Preparation of cross-linked magnetic chitosan with methionine-glutaraldehyde for removal of heavy metals from aqueous solutions, *Int. J. Environ. Anal. Chem.*, (2020) 1–17, doi: 10.1080/03067319.2020.1753718.
- [34] O.S. Amuda, A.A. Giwa, I.A. Bello, Removal of heavy metal from industrial wastewater using modified activated coconut shell carbon, *Biochem. Eng. J.*, 36 (2007) 174–181.
- [35] B. Tanhaei, A. Ayati, E. Iakovleva, M. Sillanpää, Efficient carbon interlayered magnetic chitosan adsorbent for anionic dye removal: synthesis, characterization and adsorption study, *Int. J. Biol. Macromol.*, 164 (2020) 3621–3631.
- [36] D.G. Trikkaliotis, A.K. Christoforidis, A.C. Mitropoulos, G.Z. Kyzas, Adsorption of copper ions onto chitosan/poly(vinyl alcohol) beads functionalized with poly(ethylene glycol), *Carbohydr. Polym.*, 234 (2020) 115890, doi: 10.1016/j.carbpol.2020.115890.
- [37] T.H.T. Vu, M.H. Nguyen, M.D. Nguyen, Synthesis of acidic heterogeneous catalysts with high stability based on graphene oxide/activated carbon composites for the esterification of lactic acid, *J. Chem.*, 2019 (2019) 7815697, doi: 10.1155/2019/7815697.
- [38] E.A.N. Simonetti, L. de Simone Cividanes, B.C. da Silva Fonseca, A.P.B.R. de Freitas, A. dos R. Coutinho, G.P. Thim, TiO₂-carbon composite using coconut waste as carbon source: sonocatalysis and adsorption evaluation, *Surf. Interfaces*, 12 (2018) 124–134.
- [39] G.E. Sharaf El-Deen, S.E.A. Sharaf El-Deen, Kinetic and isotherm studies for adsorption of Pb(II) from aqueous solution onto coconut shell activated carbon, *Desal. Water Treat.*, 57 (2016) 28910–28931.
- [40] A. Chaipuang, C. Phungpanya, C. Thongpoon, K. Watla-iad, P. Inkaew, T. Machan, O. Suwantong, Synthesis of copper(II) ion-imprinted polymers via suspension polymerization, *Polym. Adv. Technol.*, 29 (2018) 3134–3141.
- [41] A. Yang, P. Yang, C.P. Chin-pao Huang, Preparation of graphene oxide-chitosan composite and adsorption performance for uranium, *J. Radioanal. Nucl. Chem.*, 313 (2017) 371–378.
- [42] L.P. Hoang, H.T. Van, T.T. Hang Nguyen, V.Q. Nguyen, P.Q. Thang, Coconut shell activated carbon/CoFe₂O₄ composite for the removal of rhodamine B from aqueous solution, *J. Chem.*, 2020 (2020) 9187960, doi: 10.1155/2020/9187960.
- [43] H. Zang, Y. Li, Y. Li, L. Chen, Q. Du, K. Zhou, H. Li, Y. Wang, L. Ci, Adsorptive removal of cationic dye from aqueous solution by graphene oxide/cellulose acetate composite, *J. Nanosci. Nanotechnol.*, 19 (2019) 4535–4542.
- [44] H.N. Tran, S.-J. You, A. Hosseini-Bandegharai, H.-P. Chao, Mistakes and inconsistencies regarding adsorption of contaminants from aqueous solutions: a critical review, *Water Res.*, 120 (2017) 88–116.
- [45] H.J. Choi, Assessment of the adsorption kinetics, equilibrium and thermodynamic for Pb(II) removal using a hybrid adsorbent, eggshell and sericite, in aqueous solution, *Water Sci. Technol.*, 79 (2019) 1922–1933.
- [46] R.K. Ramakrishnan, V.V.T. Padil, S. Wacławek, M. Černík, R.S. Varma, Eco-friendly and economic, adsorptive removal of cationic and anionic dyes by bio-based karaya gum-chitosan sponge, *Polymers (Basel)*, 13 (2021) 1–20.
- [47] N.S. Abdul Mubarak, T.W. Chuan, H.P. Khor, A.H. Jawad, L.D. Wilson, S. Sabar, Immobilized Fe-loaded chitosan film for Methyl orange dye removal: competitive ions, reusability, and mechanism, *J. Polym. Environ.*, 29 (2021) 1050–1062.

- [48] F. Gu, J. Geng, M. Li, J. Chang, Y. Cui, Synthesis of chitosan-ignosulfonate composite as an adsorbent for dye and metal ions removal from wastewater, *ACS Omega*, 4 (2019) 21421–21430.
- [49] D. Banerjee, U. Sarkar, S. Chakraborty, D. Roy, Removal of a cationic bisbiguanide using functionalized activated carbons (FACs), *Process Saf. Environ. Prot.*, 92 (2014) 957–972.
- [50] M.T. Aswani, M.V. Pavan Kumar, A novel water hyacinth based biosorbent for 2,4-dichlorophenoxyacetic acid (2,4-D) removal from aqueous solution, *Desal. Water Treat.*, 165 (2019) 163–176.
- [51] I.A.W. Tan, A.L. Ahmad, B.H. Hameed, Adsorption isotherms, kinetics, thermodynamics and desorption studies of 2,4,6-trichlorophenol on oil palm empty fruit bunch-based activated carbon, *J. Hazard. Mater.*, 164 (2009) 473–482.
- [52] W. Chen, J. Luan, X. Yu, X. Wang, X. Ke, Preparation of core-shell structured polystyrene@graphene oxide composite microspheres with high adsorption capacity and its removal of dye contaminants, *Environ. Technol. (United Kingdom)*, 42 (2021) 3840–3851.
- [53] H. Dai, Y. Huang, H. Huang, Eco-friendly polyvinyl alcohol/carboxymethyl cellulose hydrogels reinforced with graphene oxide and bentonite for enhanced adsorption of Methylene blue, *Carbohydr. Polym.*, 185 (2018) 1–11, doi: 10.1016/j.carbpol.2017.12.073.
- [54] W. Zhu, X. Jiang, F. Liu, F. You, C. Yao, Preparation of chitosan-graphene oxide composite aerogel by hydrothermal method and its adsorption property of Methyl orange, *Polymers (Basel)*, 12 (2020) 2169, doi: 10.3390/polym12092169.